Density Functional Theory Investigation of the Electronic Structure and Spin Density Distribution in Peroxyl Radicals

Michael J. Raiti and Michael D. Sevilla*

Department of Chemistry, Oakland University, Rochester, Michigan 48309

Received: August 25, 1998; In Final Form: November 25, 1998

The electronic structure and spin density distribution of peroxyl radicals are investigated by density functional theory (DFT) at the B3LYP level. Results found for superoxide anion and *tert*-butyl peroxyl radicals at a variety of basis sets suggest that 6-31G is the most appropriate basis set for calculation of hyperfine coupling constants (hfcc's) of carbon-based peroxyl radicals. Calculation of parallel ^{17}O hfcc's [$A_{||}(^{17}O)$] for a series of substituted methyl peroxyl radicals with the 6-31G basis set yielded calculated values with a maximum deviation of 2.2% from experiment. Spin density distributions estimated from experiment $A_{||}(^{17}O)$ are compared to theoretical estimates from Mulliken orbital population analysis. Electronegative substitution at the carbon alpha to the peroxyl group results in an increase of terminal oxygen hyperfine coupling and spin density, shortening of C−O, and lengthening of O−O. In cases involving significant steric hindrance, however, C−O bond shortening was prevented. $A_{||}(^{17}O)$ values for the terminal peroxyl oxygen atom correlate well with Taft σ^* substitutent parameters for the R group in the peroxyl radicals (ROO$^\bullet$). Thiyl peroxyl radicals are reinvestigated using B3LYP for comparison to previous theoretical work at UHF level. This resulted in confirmation that the effect of the addition of an electron pair donor (hydroxide ion) to $CH_3SOO^\bullet$ is to alter the spin density distribution in the peroxyl group. Structural models of lipid peroxyl radicals show that vinyl peroxyl radicals may be distinguished from saturated, allylic, and ester-based peroxyl radicals on the basis of hyperfine coupling constants.

Introduction

Peroxyl radicals are well recognized as being significant to the chemistry of living systems.[1−11] Most carbon-centered free radicals formed by normal oxidative processes readily react with molecular oxygen to form peroxyl radicals.[7,12] Peroxyl radicals are relatively long-lived species that show far more selectivity than shown by hydroxyl or alkoxyl radicals.[8,13] They are, therefore, damaging to specific sites on biomolecules.[14] The importance of peroxyl radicals in living systems and their suggested involvement in a variety of disease processes[8] has stimulated a number of theoretical studies of their the structure and reactivity.[1,4−6,13,15,16] Post Hartree−Fock ab initio approaches are able to provide accurate values in comparison to experimental for parameters such as geometry, harmonic vibrational frequency, dipole moments, and hyperfine couplings,[17] but only through the inclusion of high correlation recovery and the use of large, balanced basis sets, both of which are time expensive.[13,18] Recently, the use of density functional theory (DFT) has facilitated such investigations.[13,16] DFT, which is much less time expensive than post Hartree−Fock methods, provides values that are comparable to high level ab initio calculations (such as MP2) for parameters such as equilibrium geometries,[19] vibrational frequencies,[20] and hyperfine coupling constants.[13] Several investigators[18,21] have reported that the hybrid B3LYP density functional scheme (in Gaussian 94 code), which includes Hartree−Fock exchange, is to be preferred over other functional schemes for bond dissociation energies[15] and hyperfine coupling constants (hfcc's)[13] of both peroxyl and nonperoxyl radicals. The PWP86 scheme has also been reported to provide good results in de Mon code.[17] Additionally, it has been reported that the use of large basis sets with B3LYP does not improve values over the use of smaller basis sets.[18,20] These studies have found 6-31G* to be an optimal basis when considering accuracy and expense,[16,18,20] although smaller basis sets, such as 6-31G and 4-31G, were not included in the comparisons.

This paper focuses on the spin density distribution in carbon-based peroxyl radicals. The spin density is a parameter critical to the understanding of the electronic structure of peroxyl radicals as well as their reactivity. In this work optimized geometries and hfcc's are calculated at B3LYP at a wide variety of basis sets, including the smaller basis sets 4-31G and 6-31G. The use of ^{17}O hfcc's of peroxyl atoms to estimate the electron spin density distribution on the peroxyl oxygen atoms has been suggested by Sevilla et al.[7] In this work we compare spin density distributions on the peroxyl groups for several of the peroxyl radicals determined by this approach to those obtained using Mulliken gross orbital population calculations. As a result of this comparison, we suggest correction terms to improve the estimation of spin density distribution on the peroxyl oxygen atoms by use of ^{17}O hfcc's.

The effect of electronegative substitution at the α-carbon of peroxyl radicals was investigated by Sevilla et al.[7] This previous work suggested a linear relationship between the anisotropic hyperfine coupling and the spin density in the p orbitals on each oxygen. In addition this previous work showed that the electron withdrawing power of the substituent group as measured by the Taft substituent parameter (σ^*) had a sizable effect on the spin distribution and the reactivity of the peroxyl radical. In the present study, we use DFT to attempt to theoretically confirm the relationship between spin density and hyperfine coupling [$A_{||}(^{17}O)$] and further test the relationship between spin density

10.1021/jp983514h CCC: $18.00 © 1999 American Chemical Society
Published on Web 03/02/1999

and the Taft σ^* parameter. Additionally, we describe the changes in geometry that accompany shifts of electron spin density distribution.

The thiyl peroxyl radical in solution was suggested by Razskazovskii et al.[22] to be dominated by a charge transfer state, $RS^+OO^{\bullet -}$, in which the positive sulfur center is stabilized by interaction with solvent electron donors. The investigation involved comparison of experimentally determined hfcc's to hfcc's calculated at UHF/6-31G*. In this present study, we use DFT to calculate the hfcc's of both the thiyl peroxyl radical and the corresponding species hydroxylated at the sulfur atom in order to develop a description based on DFT of the solvated peroxyl radical.

Experimental oxygen-17 hyperfine couplings for several lipid peroxyl radicals have been reported.[23] In this study we investigate lipid model compounds by theory in an attempt to determine whether it should be possible to distinguish experimentally between vinylic, allylic, saturated, and ester-based peroxyl radicals through use of oxygen-17 hyperfine coupling constants.

Methods

Density functional theory[24] calculations at the B3LYP level[24,25] on a Silicon Graphics computer system were performed using Gaussian 94[26] program for all molecules in this study. Spartan, from Wavefunction, Inc., was used for the graphical models shown in this work. The approach was to compare the isotropic (a_{iso}) and anisotropic (B) hfcc's of ^{17}O obtained by calculation at various basis sets to those reported experimentally for the two peroxyl ^{17}O atoms of peroxyl radicals.[27] The radicals were optimized at each basis set, and then calculations at that same basis set were performed for the isotropic and anisotropic ^{17}O hfcc's. These values, along with $A_{||}$ values ($A_{||} = a_{iso} + 2B$)[7] for the two peroxyl oxygen atoms, were compared to experimental values previously reported for superoxide anion radical by Sevilla et al.[7] and for *tert*-butyl peroxyl radical by Howard[28] and Wetmore et al.[13]

6-31G was selected for further study, on the basis of its accuracy in comparison to the experimental ^{17}O hfcc's for superoxide anion and *tert*-butyl peroxyl radicals. A number of peroxyl radicals with experimentally determined $A_{||}(^{17}O)$ values were then investigated employing this basis set. The appropriateness of B3LYP/6-31G for estimation of the isotropic and anisotropic hfcc's of peroxyl ^{17}O atoms was assessed by the determination of the deviation of the computed values from the experimental values for the peroxyl radicals in this study.

Results and Discussion

Superoxide Anion Radical and *tert*-Butyl Peroxyl Radical. The isotropic (a_{iso}) and anisotropic (B) ^{17}O hfcc's and $A_{||}(^{17}O)$ values for superoxide anion radical and *tert*-butyl peroxyl radical were calculated using over 15 basis sets at B3LYP level after geometry optimization at the respective basis sets. The basis sets included small basis sets [3-21G, 4-31G], moderate basis sets [6-31G (including those with plus functions and extra sets of orbitals on hydrogen and polarization functions (*)), D95v], and the CEP-121G and cc-pV5Z basis sets. The computed values are tabulated and presented as Supporting Information. The calculated isotropic ^{17}O hfcc's varied significantly from experiment according to the basis set employed, whereas the calculated anisotropic ^{17}O hfcc's, in general, were consistent and in good agreement with experimental values for nearly all basis sets (except 3-21G), as found in previous work.[13] Inclusion of polarization functions (*) in the basis set and diffuse functions, in general, resulted in poorer hfcc's in comparison to experimental values.[29,30] The 6-31G* basis set used in a previous study of peroxyl radicals[13] was found to be in poorer overall agreement with experiment than the smaller 6-31G basis set. Isotropic and anisotropic ^{17}O hfcc's were best predicted by 6-31G which showed exceptional agreement with experimental values with an average deviation from experiment of about 3%.

The effect of addition of a diffuse (+) function to the basis set was studied for the following four basis sets: 6-31G, 6-31G*, 6-311G, and 6-311G* (given in Supporting Information). Surprisingly, the effect of the diffuse function was, in most instances, to increase the magnitude of the isotropic hfcc's (^{17}O). The most significant effect was for 6-31G-type basis sets (2.6 G increase for 6-31+G over 6-31G and 4.6 G increase for 6-31+G* over 6-31G*). The addition of the diffuse function in 6-31+G* improved the prediction of the magnitude of isotropic ^{17}O hfcc's as compared to 6-31G*, but its values were still poorer than those from 6-31G. The effect of the diffuse function on the anisotropic ^{17}O hfcc's was less significant than for the isotropic ^{17}O hfcc's. Changes of anistropic ^{17}O hfcc's for all basis sets were an increase of magnitude by less than 1 G.

On the basis of the calculated ^{17}O hfcc's generated for superoxide anion radical and *tert*-butyl radical by using various basis sets, we found 6-31G to provide the best overall estimate of experimental ^{17}O hfcc's and selected it for further investigation of other peroxyl radicals.

Peroxyl Radicals at 6-31G Basis Set. The results for the various peroxyl radicals using 6-31G are summarized in Table 1. Included are the deviations of the calculated hfcc's from experimental values of the compounds for which the experimental values are known.[7] For each radical, 6-31G tends to overestimate the magnitude of $A_{||}(^{17}O)$ for the terminal oxygen atom but, also, tends to underestimate $A_{||}$ for the internal oxygen atom. This results in a negligible deviation of calculated $\Sigma A_{||}(^{17}O)$ values from experimental, even for molecules involving chlorine atoms. For all radicals investigated, the greatest deviation of $\Sigma A_{||}$ was no more than 2.2%.

A comparison of calculated hfcc's with experimental values is shown in Figure 1. The graph plots the terminal peroxyl oxygen atom $|A_{||}|$ from calculation (B3LYP/6-31G) against that from experiment.[7] All data points are within ± 1 G of the best-fit line. Clearly, calculated hfcc's can be accurately scaled to experiment.

Substitution on the carbon alpha to the peroxyl group with electronegative groups results in an increase of $A_{||}(^{17}O)$ on the terminal oxygen and a decrease of $A_{||}(^{17}O)$ on the internal oxygen (see Table 1). Both the isotropic and anisotropic hfcc's for the terminal oxygen atom increase, while both of these values for the internal oxygen atom decrease, as electronegative substituents are substituted. These observations are evident by the trends for the terminal and internal peroxyl oxygen atoms in Table 1 as the number of chlorine atoms is increased from 0 to 3, as well as by the inclusion of fluorine atoms in the radical.

Spin Densities. In general, for any peroxyl radical, the distribution of spin density from hfcc's on ^{17}O can be approximated by assuming that hfcc's which are assigned to an atom of the radical are proportional to the spin density on that atom. For atom (1),

TABLE 1. Calculated[a] and Experimental[b] Hyperfine Couplings of Peroxyl Radicals

	$a_{iso}(1)$	$a_{iso}(2)$	SUM a_{iso}	$B_{cc}(1)$	$B_{cc}(2)$	SUM B_{cc}	$A_{\|\|}(1)$	$A_{\|\|}(2)$	SUM $A_{\|\|}$	S^2
$OO^{\bullet-}$										
calcd	−21.94	−21.94	−43.89	−53.63	−53.63	−107.25	−75.57	−75.57	−151.14	0.753
expt[b]	−21	−21	−42	−56.3	−56.3	−112.6	−77.3	−77.3	−154.6	
% dev[c]	**4.5%**	**4.5%**	**4.5%**	**−4.8%**	**−4.8%**	**−4.8%**	**−2.2%**	**−2.2%**	**−2.2%**	
$HOCH_2OO^{\bullet}$	−27.77	−16.35	−44.12	−74.36	−36.21	−110.57	−102.13	−52.56	−154.70	0.753
							−94.8	−56.8	−151.6	
							7.7%	**−7.5%**	**2.0%**	
$NCCH_2OO^{\bullet}$	−28.05	−15.90	−43.95	−75.43	−36.35	−111.77	−103.47	−52.25	−155.72	0.753
							−98.4	−57.2	−155.6	
							5.2%	**−8.7%**	**0.0%**	
$(CH_3)_3COO^{\bullet}$	−27.70	−16.73	−44.43	−72.88	−37.62	−110.50	−100.58	−53.35	−153.94	0.753
	−21.8	−16.4	−38.2	−72.2	−42.6	−115.7	−94.0	−59.0	−153.9	
	27.0%	**2.0%**	**16.3%**	**0.9%**	**−11.7%**	**−4.5%**	**7.0%**	**−9.6%**	**0.0%**	
$CClH_2OO^{\bullet}$[d]										
anti	−27.52	−16.04	−43.56	−75.07	−35.83	−110.90	−102.59	−51.87	−154.45	0.753
							−97.5	−55.5	−153.0	
							5.2%	**−6.5%**	**1.0%**	
syn	−28.03	−16.29	−44.32	−75.59	−36.10	−111.69	−103.62	−52.38	−156.01	0.753
							−97.5	−55.5	−153.0	
							6.3%	**−5.6%**	**2.0%**	
$CCl_2HOO^{\bullet}$	−28.08	−14.48	−42.56	−78.02	−32.03	−110.05	−106.10	−46.50	−152.61	0.753
							−100.8	−51.3	−152.1	
							5.3%	**−9.4%**	**0.3%**	
$CCl_3OO^{\bullet}$	−28.52	−12.94	−41.46	−80.06	−28.97	−109.03	−108.58	−41.91	−150.49	0.753
							−102.6	−49.2	−151.8	
							5.8%	**−14.8%**	**−0.9%**	
$CClF_2CClFOO^{\bullet}$	−28.77	−11.99	−40.76	−81.62	−27.83	−109.45	−110.39	−39.82	−150.21	0.753
							−105	−45.2	−150.2	
							5.1%	**−11.9%**	**0.0%**	
$CF_3CF_2OO^{\bullet}$	−28.86	−11.51	−40.36	−82.99	−26.82	−109.81	−111.84	−38.33	−150.17	0.753

[a] Geometry optimizations and hfcc calculations at B3LYP/6-31G. [b] Ref 7. [c] % dev = (exp − calcd)/exp. [d] Anti and syn refer to conformers described by the relationship of Cl to the peroxyl group.

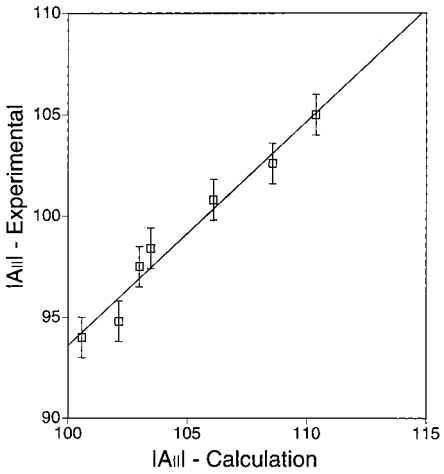

Figure 1. Comparison of the magnitude of $A_{||}$ (terminal oxygen) from experiment to that from calculation. Geometry optimizations and hyperfine coupling constants calculations were performed at B3LYP/6-31G. The radicals included in the plot are $HOCH_2OO^{\bullet}$, $NCCH_2OO^{\bullet}$, $(CH_3)_3COO^{\bullet}$, $CClH_2OO^{\bullet}$, $CCl_2HOO^{\bullet}$, $CCl_3OO^{\bullet}$, and $CClF_2CClFOO^{\bullet}$. The experimental values are from ref 7. The equation of the line is $y = 1.11x - 16.9$.

$$\rho(a_{iso})(1) = \frac{a_{iso}(1)}{a_{iso}(1) + a_{iso}(2)} \quad (1a)$$

$$\rho(B_{cc})(1) = \frac{B_{cc}(1)}{B_{cc}(1) + B_{cc}(2)} \quad (1b)$$

$$\rho(A_{||})(1) = \frac{A_{||}(1)}{A_{||}(1) + A_{||}(2)} \quad (1c)$$

where ρ is the spin density, a_{iso} is the isotropic hfcc, B_{cc} is the anisotropic hfcc, and $A_{||} = a_{iso} + 2B_{cc}$.

Peroxyl radicals have the spin density localized chiefly to the p_z orbitals of the peroxyl oxygen atoms. The Mulliken orbital

TABLE 2. Calculated Spin Densities of Peroxyl Radicals[a]

	from theory				from experiment[c]	
peroxyl radical	ρ $(a_{iso})^b$	ρ $(B_{cc})^b$	ρ $(A_{\|\|})^b$	Mulliken	ρ (a_{iso})	ρ $(A_{\|\|})$
$OO^{\bullet-}$	0.5	0.5	0.5	0.5	0.5	0.5
	0.5	0.5	0.5	0.5	0.5	0.5
$(CH_3)_3COO^{\bullet}$	0.62	0.66	0.65	0.69	0.57	0.61
	0.38	0.34	0.35	0.29	0.43	0.39
$HOCH_2OO^{\bullet}$	0.63	0.67	0.66	0.71		0.63
	0.37	0.33	0.34	0.28		0.37
$NCCH_2OO^{\bullet}$	0.64	0.675	0.66	0.71		0.63
	0.36	0.325	0.34	0.27		0.37
$CClH_2OO^{\bullet}$[d]	0.63	0.68	0.66	0.71		0.64
	0.37	0.32	0.34	0.27		0.36
$CCl_2HOO^{\bullet}$	0.66	0.71	0.695	0.74		0.66
	0.34	0.29	0.305	0.24		0.34
$CCl_3OO^{\bullet}$	0.69	0.73	0.72	0.76		0.68
	0.31	0.27	0.28	0.21		0.32
$CClF_2CClFOO^{\bullet}$	0.71	0.75	0.735	0.78		0.70
	0.29	0.25	0.265	0.20		0.30
$CF_3CF_2OO^{\bullet}$	0.715	0.76	0.745	0.79		
	0.285	0.24	0.255	0.19		

[a] Geometry optimizations, hfcc, and Mulliken population calculations at B3LYP/6-31G. [b] ρ was determined by eq 1 (in text); hyperfine coupling values are given in Table 3. [c] Experimental values determined from measurements given in ref 7. ρ determined using eq 1. [d] Values for anti and syn conformers were averaged.

calculations suggest that about 98% of the spin is localized on the $2p_z$ oxygen π-type atomic orbitals for peroxyl radicals considered in this work (with the exception of the thiyl and vinyl peroxyl radicals which are treated later).

Comparison was made in an attempt to find possible corrections for spin densities determined using calculated hfcc's that would allow for a more accurate description of actual spin densities of peroxyl oxygen atoms. Spin density, ρ, values (see Table 2) for the two peroxyl oxygen atoms were estimated using a_{iso}, B_{cc}, and $A_{||}$ calculated at B3LYP/6-31G from Table 1; Mulliken gross orbital population analysis[31] at B3LYP/6-31G;

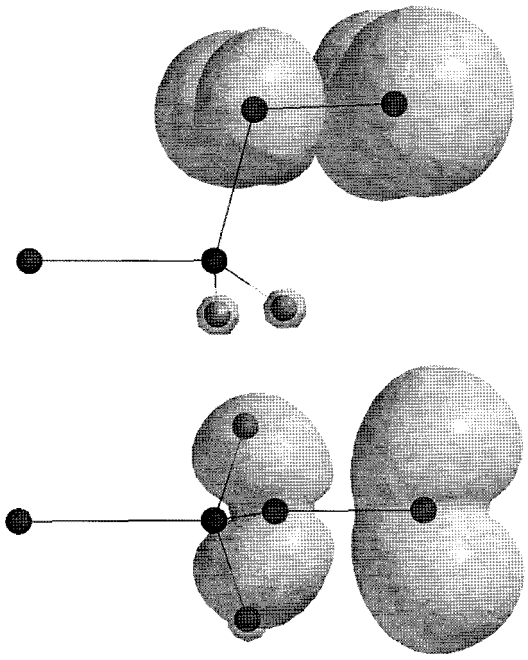

Figure 2. Spatial spin density distribution in chloromethyl peroxyl radical from calculation at B3LYP/6-31G (contour density = 0.002). The top picture shows small amounts of spin density localized on the hydrogen atoms. The overall π^* nature of the SOMO is apparent.

and a_{iso} and $A_{||}$ from experimental data all given in Table 1. Comparisons were made of the spin densities obtained by the first three estimations (eqs 1a−c) to the spin densities predicted by the Mulliken analysis in order to evaluate each of the three methods as estimates of spin density. See Figure 2 for spin density distribution of a typical substituted methyl peroxyl radical.

$\rho(B_{cc})$ from eq 1b is a direct estimate of spin density in a p_z orbital. The dipolar interaction between the unpaired electron and the nucleus results in the anisotropic coupling and has a $1/r^3$ dependence. This results in the contribution from neighboring atoms to the dipolar coupling being small in comparison to that from the p_z orbital of the atom itself. $\rho(a_{iso})$ from eq 1a gives a less accurate estimate due to substantial next neighbor couplings through spin polarization and other mechanisms. Finally, since $A_{||}$ largely weights B over a_{iso}, $\rho(A_{||})$ should be a reasonable estimate of the spin density in the p orbitals. As expected, for each radical in Table 2, $\rho(B_{cc})$ is closest to the Mulliken analysis of the three methods followed closely by $\rho(A_{||})$.

Experimental spin densities are most conveniently estimated from experimental $A_{||}$ values. Therefore, to test the accuracy of such estimates from $A_{||}$ couplings, we compared theoretical $\rho(A_{||})$ (eq 1c) and Mulliken spin density values. In general, we find a good correlation with the theoretical $\rho(A_{||})$ for the terminal peroxyl only 0.04−0.05 lower than the Mulliken analysis, and that for the internal oxygen atom about 0.06−0.07 higher than the Mulliken analysis. An approximate correction of $\rho(A_{||})$ to the Mulliken values is then to add 0.04−0.05 to the spin density value for the terminal oxygen atom and to subtract 0.06−0.07 from the spin density value for the internal oxygen atom.

It was noted above that substitution of electronegative groups on the carbon to which the peroxyl group is attached increases isotropic hfcc's, anisotropic hfcc's, and $A_{||}(^{17}O)$ values for the terminal oxygen atom and decreases these values for the internal oxygen atom. Since the values in the first three columns of Table 2 were obtained by use of eq 1, there are similar trends in spin density. These trends are consistent with values estimated from experimental[7] couplings.

SCHEME 1

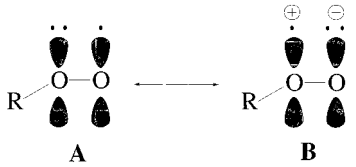

Effect of Electronegative Substitution on Spin Distribution and Geometry. Next we consider the effect of substituents on the spin density distribution and geometry in peroxyl radicals. The important resonance forms for peroxyl radicals are shown in Scheme 1.

For valence structure **A** in Scheme 1, the unpaired electron is localized on the terminal oxygen atom, whereas in **B** it is localized on the internal oxygen atom with a formal positive charge on the inner oxygen atom. The electron density of the internal oxygen atom is, therefore, substantially greater in **A** than in **B**, and thus, **A** provides greater stabilization than **B** for electron withdrawing groups, while electron donating groups would tend to stabilize **B**. This trend is evident in Table 1 by comparison of hfcc's for the various radicals as electronegative substitution is increased.

Changes in geometry with electronegative substitution are shown in Figure 3. In general, as the number of chlorine atoms increases, the C−O bond distance shortens, while the O−O bond distance lengthens. Additionally, as the electronegativity of the α-carbon substituents increases, the contribution of electron density from the internal oxygen atom becomes more significant, and therefore, the unpaired spin density on the peroxyl group becomes more localized on the terminal oxygen atom, as with **A** in Scheme 1. Also, as the C−O bond shortens and becomes more ionic in nature, the O−O bond weakens and lengthens due to lowering of its ionic character.

However, for the trichloromethyl peroxyl radical, the C−O bond is lengthened and the O−O bond is shortened compared to that in the dichloromethyl peroxyl radical. This cannot be explained by considering only electronic effects. Molecular models (Figure 3) show that steric interactions involving the terminal oxygen atom may be significant in some of the radicals, as is especially evident when comparing ∠C−O−O for *tert*-butyl peroxyl to that for the chlorinated peroxyl radicals. In general, as seen in Figure 3, the angle is greatest for radicals with three bulky groups on the carbon: *tert*-butyl peroxyl (112.6°) and trichloromethyl peroxyl (112.7°). For radicals with less than three bulky groups, the ∠C−O−O is smaller (108.4° to 110.6°) owing to diminished steric interactions.

Figure 4 plots $|A_{||}|$ for the terminal peroxyl oxygen atom against the Taft substituent parameter (σ^*) which is a measure of the electron withdrawing power of the substituent. The upper line is from calculations performed in this study, while the lower line shows experimental values from previous experimental work.[7] The graph shows a strong correlation between both calculated and experimental $A_{||}(^{17}O)$ values with σ^*. The slopes of the experimental and theoretical lines are within 10% of each other (3.37 for experimental vs 2.99 for calculated). The overestimation (translation along y-axis) of $A_{||}$ for the terminal oxygen atom by the B3LYP/6-31G calculation is about 6−7 G.

Thiyl Peroxyl Radical. Razskazovskii et al.[22] performed experimental and theoretical studies of thiyl peroxyl radical ($RSOO^{\bullet}$) and showed that $RSOO^{\bullet}$ has a highly variable spin distribution that in aqueous solution differs in nature from

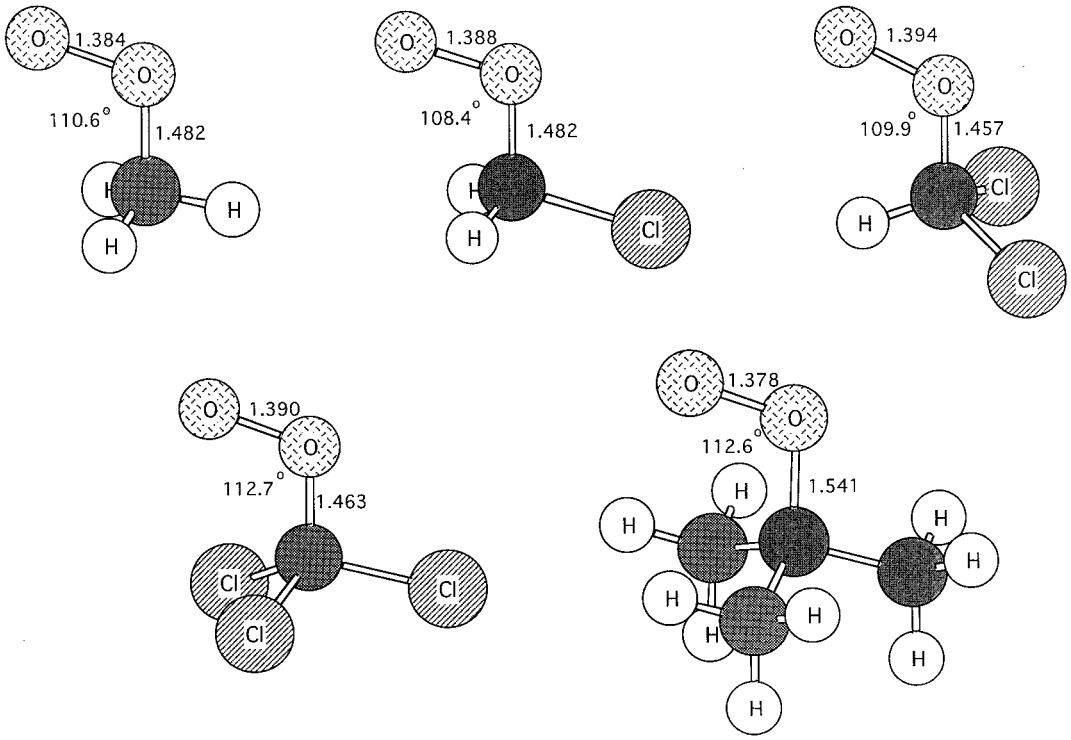

Figure 3. Geometries of methyl and substituted methyl peroxyl radicals. Geometry optimizations were performed at B3LYP/6-31G.

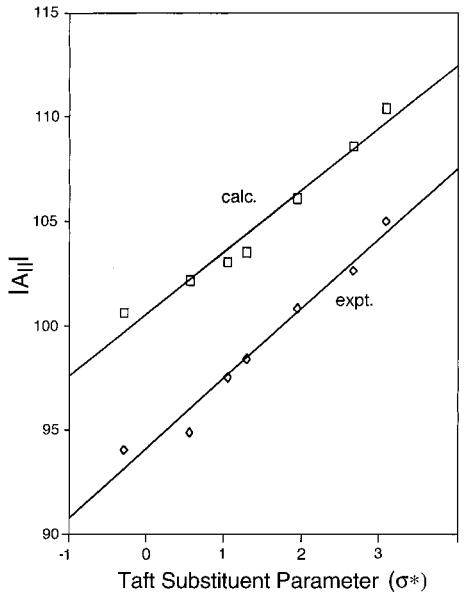

Figure 4. Calculated $|A_{||}(^{17}O)|$ vs σ^* for the terminal peroxyl oxygen atom of peroxyl radicals which include electronegative substituents. $|A_{||}(^{17}O)|$ is from hfcc's from radicals optimized at B3LYP/6-31G. The radicals that are included in the plot are the same as those in Figure 1. Experimental values are given in ref 7. Equations of the lines are $y = 2.99x + 100.5$ for the top line (calculated) and $y = 3.37x + 94.1$ for the bottom line (experimental).

carbon-based peroxyl radicals, but that in some nonpolar systems has a similar distribution to carbon-based peroxyl radicals. These experimental findings showed that the spin density of $RSOO^{\bullet}$ in aqueous environment was more evenly distributed in the peroxyl group than is generally found for carbon-based peroxyl radicals. For *tert*-butyl peroxyl radical, a typical carbon-based peroxyl radical, the hfcc's on the peroxyl group are −94 G for the terminal oxygen atom and −59 G for the internal oxygen atom. For $t\text{-}C_4H_7SOO^{\bullet}$, the hfcc's were found by Razskazovskii et al. to be −79 and −61 G for the terminal and internal oxygen

TABLE 3. Hyperfine Couplings of Thiyl Peroxyl Radicals

	$CH_3SOO^{\bullet}$			$CH_3S(OH)OO^{\bullet-}$		
	6-31G[a]	6-31G*[a]	expt[b]	6-31G[a]	6-31G*[a]	expt[b]
isotropic						
O(17)	−27.54	−16.80		−25.38	−15.98	
O(17)	−12.79	−10.76		−23.07	−15.90	
sum	−40.33	−27.56		−48.46	−31.88	
anisotropic						
O(17)	−66.46	−66.70		−60.55	−60.54	
O(17)	−40.50	−41.78		−46.28	−48.06	
sum	−107.96	−108.48		−108.60	−108.60	
$A_{||}(1)$	−94.01	−83.50	−96	−85.93	−76.52	−81
$A_{||}(2)$	−53.29	−52.54	−51	−69.36	−63.97	−62
sum $A_{||}$	−147.29	−136.04	−147	−155.29	−140.48	−143

[a] Geometry optimizations and hfcc calculations both at this basis set using B3LYP. [b] Ref 22.

atoms, respectively, in a methanol−water glass, but −96 and −51 G in a Freon matrix. The large change in spin distribution with matrix is quite unusual and suggested a specific interaction with an electron donor acting as a Lewis base at the sulfur atom.

Theoretical calculations were also carried out by Razskazovskii et al. at UHF/6-31G* to investigate the effect of electron donors at the sulfur atom in $RSOO^{\bullet}$ using hydroxyl ion as the model donor ($CH_3S(OH)OO^{\bullet-}$. In the present study, we repeated the calculations on $RSOO^{\bullet}$ and $RS(OH)OO^{\bullet-}$ using density functional theory in order to check previous results obtained using UHF/6-31G*. The results we obtained confirmed the description previously found based upon UHF calculations. Hfcc's for $CH_3S(OH)OO^{\bullet-}$ and $CH_3SOO^{\bullet}$ were calculated using a variety of basis sets at B3LYP (data not shown), which were variations of 6-31G and included a combination of diffuse function (+ and ++), polarization (* and **), and an additional p orbital on H atoms (e.g., 6-311G). 6-31G provided an excellent match to experimental values for uncomplexed $CH_3SOO^{\bullet}$, although it performed less well in comparison of $CH_3S(OH)OO^{\bullet-}$ to experimental values of aqueous (complexed) $CH_3SOO^{\bullet}$ (see Table 3). This poor performance of the complexed species may

TABLE 4. Calculated Spin Densities[a] of Thiyl Peroxyl and Model Lipid Peroxyl Radicals[b]

	$CH_3SOO^{\bullet}$	$CH_3S(OH)OO^{\bullet-}$	*cis* 3-pentenyl-2-peroxyl radical	pentanyl-3-peroxyl radical	methylbutyrate-alpha-peroxyl radical	*cis* 2-pentene-3-peroxyl radical	*trans* 2-pentene-3-peroxyl radical
S	0.05	0.01					
O	0.62	0.56	0.69	0.69	0.70	0.61	0.61
O	0.32	0.42	0.29	0.29	0.28	0.27	0.27
C2						0.18	0.17

[a] In the p_z orbital. [b] Mulliken orbital population analysis at B3LYP/6-31G.

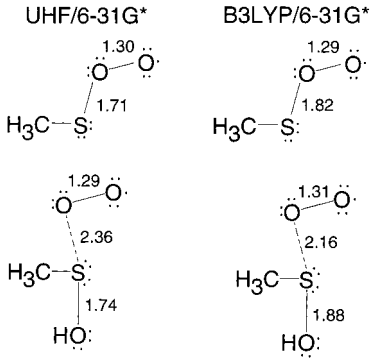

Figure 5. S−OO, S−OH, and O−O bond distances for thiyl peroxyl and hydroxylated thiyl peroxyl radicals from UHF and DFT. UHF structures are from ref 22. DFT structures are from this work and were optimized with B3LYP/6-31G*.

be explained as being due to the hypervalent sulfur in $CH_3S(OH)OO^{\bullet-}$ which necessitates the use of polarization (d orbitals) in the basis set employed. As expected, calculations of the $CH_3S(OH)OO^{\bullet-}$ radical performed using 6-31G* produced values in better agreement with the experiment than those at 6-31G.

Geometry optimized structures at both UHF and B3LYP levels (Figure 5) show that the effect of the hydroxide ion interacting with the sulfur atom is to increase the length of the bond between the sulfur atom and the internal oxygen atom of the peroxyl group. The effect of the hydroxide ion on the electron density of the peroxyl oxygen atoms is to shift the density toward the terminal peroxyl oxygen atom (away from the sulfur atom) with a concomitant shift of spin density to the internal oxygen atom (Figure 5). The lengthening of the S−O bond distance upon addition of the hydroxide ion, then, should correspond to a decrease in the magnitude for the hfcc's of the terminal oxygen atom and an increase in the magnitude for the hfcc's of the internal oxygen atom. We found this indeed to be the case at B3LYP using either the 6-31G or the (6-31G*) basis set. We find that the ratio of the $A_{||}(^{17}O)$ hfcc's for terminal to internal oxygen atoms is about 1.8 (1.6) to 1 for the $RSOO^{\bullet}$, while the ratio is near 1.2 (1.2) to 1 for $RS(OH)OO^{\bullet-}$ versus experimental values, 1.9 to 1 for the $RSOO^{\bullet}$, and 1.3 to 1 for $RS(OH)OO^{\bullet-}$ (see Table 4).

Models of Lipid Peroxyl Radicals. Our study of peroxyl radicals was extended to include models of lipid peroxyl radicals that may be formed through oxidative damage in lipid systems. Experimental anisotropic hfcc's for several lipid peroxyl radicals have been reported by Sevilla et al.[23] It is of interest to use theoretical calculations to ascertain if differences in experimental ^{17}O hfcc's for various types of peroxyl radicals may be useful in classifying these species. The lipid models investigated were cis 3-pentenyl-2-peroxyl radical, pentanyl-3-peroxyl radical, methyl butyrate-α-peroxyl radical, cis 2-pentene-3-peroxyl radical, and trans 2-pentene-3-peroxyl radical (see Figure 6). B3LYP/6-31G was chosen as the basis set on the basis of the results reported above for superoxide anion and *tert*-butyl peroxyl radicals. Vinylic peroxyl radicals substantially differed from the other model radicals in isotropic and anisotropic hfcc's for the terminal oxygen atom (see Table 5). The calculated terminal oxygen $A_{||}(^{17}O)$ values are 10−11 G smaller than the other peroxyl radicals and, since these are experimentally measured, this large difference would be easily observed. The reason for the smaller coupling is a substantial delocalization of the spin density from the terminal oxygen of the peroxyl group to the vinyl carbon as depicted in the simplified valence structures shown below.

$$CH_2{=}CH_2{-}O{-}O^{\bullet} \leftrightarrow {}^{\bullet}CH_2{-}CH_2{=}O^{+}{-}O^{-}$$

The spin density on the terminal vinyl carbon in this radical is 0.18. This suggests that hfcc's would be useful for distinguishing vinylic peroxyl radicals from the other types of radicals investigated, although it would be difficult to distinguish saturated peroxyl, allylic peroxyl, or ester-based peroxyl radicals from one another.

Conclusion

Our results show that use of the smaller 6-31G basis set gives experimental hfcc's that more closely match experimental peroxyl radical values than do large basis sets in agreement with previous work by Wetmore et al.[13] and Cohen and Chong.[18] Wetmore et al. suggest that the fact that smaller basis sets yield better results than larger basis sets is a result of a cancellation of errors. The work of Cohen and Chong indicates that improvements that are expected for larger basis sets from increased flexibility are negated in DFT by correlation effects. Wetmore et al. found in their study that decontraction of 6-31G-(d,p) results in poorer results for hfcc's of *tert*-butyl peroxyl radical. This led them to suggest that the success of 6-31G-type basis sets results from the contraction scheme. Wetmore et al. reported poor results for $FOO^{\bullet}$, which has a strongly electrognegative group attached directly to the peroxyl radical.

The only radicals in common with ours in the study of Wetmore et al. are the *tert*-butyl and chloromethyl peroxyl radicals, and the only basis set in common was 6-31G(d,p). For this basis set, our values match theirs closely but with a consequence of slightly different geometries resulting from optimization at different levels. In several other instances, their basis sets differ from ours only in that theirs contain two polarization functions, whereas ours only contain one. For these, there is little difference in the isotropic hyperfine couplings generated when the basis set included one or two polarization functions. This can also be seen in our data (Supplemental Table 2) by comparing the isotropic hyperfine couplings for 6-31G* (−17.88 and −12.93 G for the terminal and internal oxygen atoms, respectively) to those for 6-31G** (−17.88 and −12.92 G, respectively).

While we are in agreement with the estimate of "experimental" isotropic couplings for *tert*-butyl peroxyl radical by Wetmore et al., we believe their estimate of the isotropic hfcc for

TABLE 5. Hyperfine Couplings of Model Lipid Peroxyl Radicals[a]

	cis 3-pentenyl-2-peroxyl radical	methyl butyrate-alpha-peroxyl radical	pentanyl-3-peroxyl radical	*cis* 2-pentene-3-peroxyl radical	*trans* 2-pentene -3-peroxyl radical
isotropic					
O(17)	−27.52	−27.49	−27.50	−24.62	−24.74
O(17)	−16.90	−15.98	−17.25	−16.40	−16.73
anisotropic					
O(17)	−72.85	−73.97	−73.19	−65.06	−65.04
O(17)	−37.80	−36.80	−37.99	−35.09	−36.06
$A_{\|\|}(1)$	−100.37	−101.46	−100.69	−89.68	−89.79
$A_{\|\|}(2)$	−54.70	−52.78	−55.24	−51.49	−52.80
sum $A_{\|\|}$	−155.07	−154.24	−155.93	−141.16	−142.59

[a] Geometry optimizations and hfcc calculations at B3LYP/6-31G

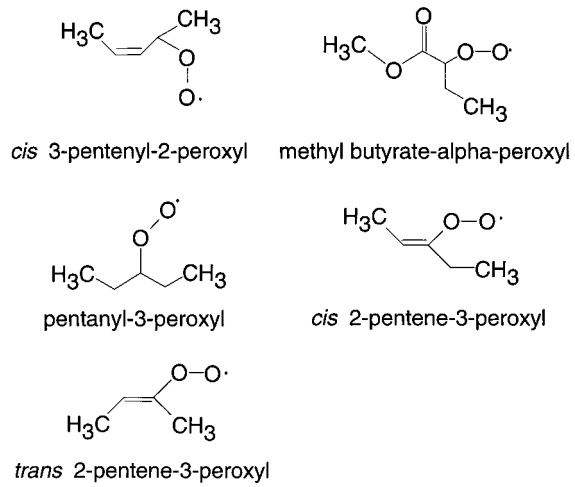

Figure 6. Structural models of lipid peroxyl radicals.

the internal oxygen atom of chloromethyl peroxyl radical of −11.1 G is incorrect. Their estimate was based on experimental $A_{||}$ couplings measured by this lab. We expect the sum of a_{iso} for the two oxygen atoms (Σa_{iso}) to be close to −38 G on the basis of the experimental values for other similar peroxyl radicals. The −11.1 G estimate results in a total substantially below this value. While our results do show that Σa_{iso} decreases slightly with increase of the electronegativity of R, the value that Wetmore et al. report for a_{iso} for the internal oxygen atom of chloromethyl peroyxl radical would require a substantially greater decrease from −38 G than can be expected to occur from electronegative substitution. Comparison of our calculations (Table 1) to experiment leads us to estimate the isotropic hfcc of the terminal oxygen atom of chloroperoxyl radical to be −22.5 G (which is close to the estimate by Wetmore et al.) and that of the internal oxygen atom to be −16 G. By using these values we find that the 6-31G basis set used in our work yields better agreement with experiment than the larger basis sets used by Wetmore et al.

For both the chloromethyl peroxyl and *tert*-butyl peroxyl radicals the O−O and C−O bond distances reported by Wetmore et al. are shorter than those reported by us. The larger basis set employed by Wetmore et al., 6-311+G(d,p), suggests that their values are likely to be more reliable for geometry.

Estimates of the spin density distribution in the peroxyl group from isotropic (a_{iso}), anisotropic (B), and parallel [$A_{||}(^{17}O)$, $A_{||} = a_{iso} + 2B$] hyperfine couplings were compared to Mulliken gross orbital population analysis spin densities at B3LYP/6-31G. It was clear that the use of anisotropic (B_{cc}) ^{17}O hfcc's or $A_{||}(^{17}O)$ is significantly better than the use of isotropic (a_{iso}) hfcc's in describing the spin density distribution.

In this work employing DFT, we find trends, which are consistent with experimental findings, which show clear evidence for the effect of electronegative substitution at the alpha carbon of methyl peroxyl radicals. As the central carbon atom of the radical is substituted with more electronegative substituents, the spin density on the terminal peroxyl oxygen atom increases with a corresponding decrease in the spin density on the internal oxygen atom. The substitution of electronegative chlorine atoms resulted in shortening of the C−O bond and lengthening of the O−O bond (Figure 3). The bond distances for trichloromethyl peroxyl radical, however, were not in agreement with these trends due to steric factors. The changes in bond distances can be explain by the stabilization of the **A** valence structure in Scheme 1 with increasing substitution of electronegative atoms. The **B** valence form has a strong O−O bond due to its ionic character. As a consequence, stabilization of the **A** form weakens the O−O bond and concomitantly strengthens the C−O bond. Chloromethyl peroxyl radicals with one or two chlorine atoms show smaller ∠COO than found for methyl peroxyl radical. However, substitution of three chlorine atoms results in larger COO bond angles than methyl peroxyl radical, likely as a result of steric factors. This is confirmed by our calculations for the *tert*-butyl peroxyl radical that yield bond angles similar to those of the trichloromethyl peroxyl radical.

The thiyl peroxyl radical was suggested in earlier work[22] to be dominated by a charge transfer state, $RS^{+}OO^{\bullet -}$, in which the positive sulfur center is stabilized by interaction with an electron donor. This conclusion is supported by our work employing density functional theory at the B3LYP level. We find that the association of the electron donor results in the near equivalency of the peroxyl oxygen spin densities as found experimentally as well as a substantial lengthening of the sulfur−peroxyl oxygen bond. Additionally, the use of model compounds for peroxyl radicals of lipids damaged by oxidation suggests that ^{17}O hfcc's would be useful in distinguishing vinylic peroxyl radicals from other types of peroxyl radicals; however, we note that, although interesting, this species is unlikely in a lipid system undergoing oxidation since its precursor would be the highly reactive vinyl radical. The calculations suggest that the more probable allylic, saturated, and alpha-ester lipid peroxyl radicals would have indistinguishable ^{17}O hfcc's.

Acknowledgment. We thank the National Cancer Institute of the National Institutes of Health (Grant RO1CA45424) and the Oakland University Research Excellence Fund for support of this work.

Supporting Information Available: Tables of hyperfine couplings and coordinates for various radicals. This material is available free of charge via the Internet at http://pubs.acs.org.

References and Notes

(1) Besler, B. H.; Sevilla, M. D.; MacNeille, P. *J. Phys. Chem.* **1986**, *90*, 6446.

(2) Merenyi, G.; Lind, J.; Engman, L. *J. Chem. Soc., Perkin Trans.* **1994**, *2*, 2251.
(3) Alfassi, Z. B.; Mosseri, S.; Neta, P. *J. Phys. Chem.* **1989**, *93*, 1380.
(4) Krauss, M.; Osman, R. *J. Phys. Chem.* **1995**, *99*, 11387.
(5) Jenkin, M. E.; Hayman, G. D. *J. Chem. Soc., Faraday Trans.* **1995**, *91*, 1911.
(6) Jonsson, M. *J. Phys. Chem.* **1996**, *100*, 6814.
(7) Sevilla, M. D.; Becker, D.; Yan, M. *Chem. Soc., Faraday Trans.* **1990**, *89*, 3279.
(8) Pryor, W. A. *Annu. Rev. Physiol.* **1986**, *48*, 657.
(9) Becker, D.; Yanez, J.; Sevilla, M. D.; Alonso-Amigo, M. G.; Schlick, S. *J. Phys. Chem.* **1987**, *91*, 492.
(10) Neta, P.; Huie, R. E.; Mosseri, S.; Shastri, L. V.; Mittal, J. P.; Maruthamutha, P.; Steenken, S. *J. Phys. Chem.* **1989**, *93*, 4099.
(11) Neta, P.; Huie, R. E.; Maruthamuthu, P.; Steeken, S. *J. Phys. Chem.* **1989**, *93*, 7654.
(12) von Sonntag, C. *The Chemical Basis of Radiation Biology*; Taylor and Francis: New York, 1987; Chapters 3 and 4.
(13) Wetmore, S. D.; Boyd, R. J.; Eriksson, L. A. *J. Chem. Phys.* **1997**, *106*, 7738.
(14) Halliwell, B.; Gutteridge, J. M. C. *Free Radicals in Biology and Medicine*; Clarendon: Oxford, U.K., 1985.
(15) Armstrong, D. A.; Yu, D.; Rauk, A. *Can. J. Chem.* **1996**, *74*, 1192.
(16) Jursic, B. S. *J. Mol. Struct. (THEOCHEM)* **1996**, *365*, 75.
(17) Eriksson, L. A. *Mol. Phys.* **1997**, *91*, 827. (Also refs 1−5 therein.)
(18) Cohen, M. J.; Chong, D. P. *Chem. Phys. Lett.* **1995**, *234*, 405.
(19) Jursic, B. S. *J. Mol. Struct. (THEOCHEM)* **1997**, *394*, 19.
(20) Stephens, P. J.; Devlin, F. J.; Chabalowsk, C. F.; Frisch, M. J. *J. Phys. Chem.* **1994**, *98*, 11623.
(21) Barone, V. *Theor. Chim. Acta* **1995**, *91*, 113.
(22) Razskazovskii, Y.; Colson, A.-O.; Sevilla, M. D. *J. Phys. Chem.* **1995**, *99*, 7793.
(23) Sevilla, M. D.; Champagne, M.; Becker, D. *J. Phys. Chem.* **1989**, *93*, 2653.
(24) Frisch, M. J.; et al. GAUSSIAN 92/DFT, Revision F. S.; Gaussian Inc.: Pittsburgh, PA, 1993.
(25) Beck, A. D. *Phys. Rev.* **1988**, *A38*, 3098.
(26) Frisch, M. J.; Trucks, G. W.; Schlegel, H. B.; Gill, P. M. W.; Johnson, B. G.; Rob, M. A.; Cheeseman, J. R.; Keith, T. A.; Peterson, G. A.; Montgomery, J. A.; Raghavachari, K.; Al-Laham, M. A.; Zakrzewske, V. G.; Oritz, J. V.; Foresman, J. B.; Ciolowshi, J.; Stefanow, B. B.; Nanayakkara, A.; Challocombe, M.; Peng, C. Y.; Ayala, P. Y.; Chen, W.; Wong, M. W.; Andres, J. L.; Replogle, E. S.; Gomperts, R.; Martin, R. L.; Fox, D. J.; Binkley, J. S.; Defrees, D. J.; Baker, J.; Stewart, J. P.; Head-Gordon, M.; Gonzalez, C.; Pople, J. A. GAUSSIAN 94 (Revision B.2); Gaussian Inc.: Pittsburgh, PA, 1995.
(27) The anisotropic hyperfine coupling constants were calculated using the modifications of links 601 and 602 in Gaussian94 by V. Barone. Included in the input keyword list was the following: PROP IOP(6/17=2, 6/26=4). This results in the computation of field gradients with the spin instead of the total electron density not including the nuclear contribution. For discussion of anisotropic hyperfine coupling constants, see ref 21.
(28) Howard, J. A. *Can. J. Chem.* **1972**, *50*, 1981.
(29) Boness, M. J. W.; Schulz, G. J. *Phys. Rev. A* **1970**, *2*, 2182.
(30) Celotta, R. J.; Bennett, R. A.; Hall, J. L.; Siegel, M. W.; Levine, J. *Phys. Rev. A* **1972**, *6*, 631.
(31) Szabo, A.; Ostlund, N. S. *Modern Quantum Chemistry*, McGraw-Hill Publishing: New York, 1989.